Toxicity assessment of laser-induced graphene by zebrafish during development

Toxicity assessment of laser-induced graphene by zebrafish during development

IOP Publishing J. Phys. Mater. 3 (2020) 034008 https://doi.org/10.1088/2515-7639/ab9522

Journal of Physics: Materials

OPEN ACCESS

RECEIVED
29 April 2020

ACCEPTED FOR PUBLICATION
20 May 2020

PUBLISHED
8 June 2020

PAPER

Toxicity assessment of laser-induced graphene by zebrafish during development

Marta d'Amora[1], **Andrea Lamberti**[1,2], **Marco Fontana**[1] **and Silvia Giordani**[1,3]

[1] Istituto Italiano di Tecnologia, Nano Carbon Materials and Center for Sustainable Future Technologies, Turin, Italy
[2] Politecnico di Torino, Dipartimento di Scienza Applicata e Tecnologia (DISAT), Turin, Italy
[3] School of Chemical Sciences, Dublin City University (DCU), Dublin, Ireland

E-mail: silvia.giordani@dcu.ie

Keywords: laser-induced graphene, few-layer graphene, toxicity, zebrafish, development

Supplementary material for this article is available online

Abstract

Laser-induced graphene (LIG) is a three-dimensional porous graphene-based material easily prepared by single or multiple laser direct writing on a polymeric or organic surface. It possesses impressive physical and chemical properties, including high surface area, hierarchical porosity, and good electrical conductivity. Here, we investigate the toxicological profile of LIG and its impact in zebrafish (*Danio rerio*) as *in vivo* biological models with high homology with humans. We evaluate the effect of LIG, administered in different concentrations to zebrafish embryos, on different biological parameters, including embryo viability and morphological changes. Our results show that LIG does not exhibit toxic effects and does not interfere with zebrafish development, even at high concentrations. Our findings provide direct evidence of the LIG biocompatibility and offer a promising avenue for its safe use in biological applications.

1. Introduction

Graphene-family nanomaterials (GFNs), including monolayer graphene, few-layer graphene (FLG), graphene oxide (GO), reduced graphene oxide (rGO), graphene nanoribbons and graphene nanosheets (GNS) [1, 2] are increasingly employed in energy harvesting and storage, electronic devices [3, 4] and biomedical applications [5–7]. However, a major concern is represented by the toxicity of these nanomaterials. Several studies assessing the *in vitro* and *in vivo* toxicity/biocompatibility of GFNs have shown their toxic effects with different degree in cultured cells and model organisms [8]. In particular, the cytotoxic effects of the different GNFs on several cell lines included mitochondrial injury, membrane integrity destruction, morphological changes, DNA damage and cell apoptosis [9–13]. Moreover, GNFs exerted developmental toxicity in zebrafish, causing growth inhibition with morphological abnormalities [14–17]. In particular, pristine graphene (170–390 nm) caused perturbations in the survival, hatching and heart beat rates with yolk sac and pericardial edema [15]. Also, GO nanosheets induced similar toxic effects in embryos and larvae [17]. Moreover, we have recently reported that a commercial graphene oxide (600 nm) induced toxicity in zebrafish at high doses, with perturbations in all the endpoints analyzed (survival, hatching, swimming, morphology) [16]. Also in mice and rats, graphene-family nanomaterials induced toxic effects, with inflammation response, leading to different effects, in particular, tissue injuries [10, 18, 19].

The toxicity of these nanomaterials have been related to several factors, such as aggregations, average and lateral size and surface area [12, 20, 21].

Laser-induced graphene (LIG) is a young member of the FLG family, first reported by Tour and coworkers in 2014 [22]. The research interest around this three-dimensional arrangement of bi-dimensional flakes is growing exponentially thanks to its peculiar properties. First, it is obtained by a fast and cost-effective direct-laser writing on flexible polymeric surfaces and it exhibits relatively high surface area, good electrical conductivity and interesting mechanical properties [23]. Moreover, it can be easily doped with several elements or decorated with oxides and dichalcogenides, in order to improve its performance in

specific applications [24–27]. In the last five years, LIG has been obtained on several different materials ranging from technical polymer (Kapton, PEEK, Kevlar) to vegetal substrates (coconut, wood, bread) enlarging its potential application to almost every technological fields [28]. Indeed, LIG has been proposed for the fabrication of strain sensors, chemical sensor, electrodes for catalysis or energy harvesting and storage devices [28–34].

It can be obtained using several laser sources with wavelenghts in the infrared, visible and UV regions. The formation mechanism was previously disclosed as depending on the absorption of the incident laser power by the polymer that induces a locally raise of the temperature causing chemical bonds to break. In this step the atoms rearrangement occurs with the formation of graphitic structure. Several species (depending on the starting polymer) evaquate the polymer network as gaseous products generating holes with different dimensions, resulting in a the characteristic foam-like morphology of LIG [35].

Moreover, the LIG composition and its surface properties can be modified following different strastegies. LIG of various compositions is formed during the laser induction process by tuning of laser parameters, changing the gas environment or acting on the substrate composition [35] In these ways it is possible to achieve different atomic ratios of carbon, nitrogen, and oxigen and modification of the LIG wettability.

Thanks to its promising biological, physicochemical, and electronic properties, LIG could be investigated as potential bio-paltforms, as well as other graphene-family nanomaterials, for different biomedical applications, such as bioimaging and cancer theranostic, tissue regenerative scaffolds, photo thermal and photodynamic treatments. In particular, its atomic 2D morphology and high surface area allow to biofuntionalize and decorate the LIG with proteins, fluorospores and other molecule for their utilization in biomedical.

Although several reports have already demonstrated the potentiality of LIG for biological applications such as electrodes for neural signal recording or stimulation [36], and their anti-biofilm activity [37], no toxicological studies have been reported so far.

For this reason, herein we present a detailed study about the toxicity of LIG investigated through zebrafish model. Zebrafish are increasingly employed as alternative model systems to assess developmental toxicity of different nanomaterials, chemicals and drugs. Zebrafish offer several advantages making them promising systems for *in vivo* high-throughput screening. A toxicity assessment in zebrafish embryos and larvae can be performed in a week; this time is short if compared with the duration of a mammalian assay. Zebrafish have small size, high fecundity and fast embryonic development. They are low cost, optically transparent and easily handled [38]. The optical transparency allows to detect the effects of nanomaterials in tissues and organs [39] and to assess different morphological endpoints by using a simple stereomicroscope [40]. Moreover, the results obtained in zebrafish can predict the nanomaterials behavior and toxicity in humans [22, 41, 41], thanks to the high homology between the two species, confirmed by the genomic sequencing [43]. In the present study, we assess the effects of LIG by analyzing the growth, hatching and development of embryos treated with different concentrations of LIG. Our results provide new insight into the toxicity/biocompatibility of graphene produced by laser writing and consequently on its potential bio-applications.

2. Methods

2.1. Materials synthesis

The electrodes were fabricated using a micromachining system produced by Microla Optoelectronics srl equipped with a CO_2 pulsed laser working at 10.6 μm wavelength, with tunable process parameters (power, pulse frequency and scan speed). The laser system is composed by beam expander (2X) and galvanometric scanner with a focusing objective of 100 mm. The operating laser parameters used in this work are: power 6 W, frequency 20 kHz, scanning rate 500 mm s^{-1}. After laser-writing LIG was manually removed by the remaining polyimide support by scratching with a razor blade, weighted in a microbalance and then finely dispersed in deionized water by 1 h of ultrasonication treatment.

2.2. Characterization

The morphology of the obtained LIG material was studied with a Zeiss Supra 40 Field-Emission Scanning Electron Microscope (Zeiss) equipped with an Oxford Si(Li) detector for Energy Dispersive X-ray analysis (EDX). Metallic coating was not required since the obtained LIG material is conductive.

Structural characterization was carried out on a FEI Tecnai G2 F20 S-TWIN Transmission Electron Microscope operated at 200 kV acceleration voltage. Concerning sample preparation, a dispersion of LIG flakes in high-purity ethanol (>99.8%) was obtained by sonication and subsequently drop-casted to a holey-carbon Cu TEM grid. The analysis of TEM images for surface area estimation was carried out with ImageJ software.

X-ray Photoelectron Spectroscopy (XPS) was performed on a PHI 5000 VersaProbe (Physical Electronics) instrument, equipped with monochromatic Al Kα radiation (1486.6 eV energy) X-ray source. Different pass energy values were used for survey (187.75 eV) and HR spectra (23.5 eV). Charge compensation during measurements was obtained with a combination of electron beam and low-energy Ar beam system. The binding energy scale was calibrated to the C-C/C-H component (284.5 eV) of the C1 s region. CasaXPS software was used for the analysis of spectra.

Size dispersion have been measured by Zetasizer Nano ZS90 (Malvern) on solutions of LIG with a concentration of 0.05 mg ml^{-1}.

2.3. In vivo toxicity protocol

Zebrafish maintenance and spawning followed the conditions previously described [44]. Briefly, wild-type zebrafish were kept under controlled conditions and were fed twice a day. Embryos, obtained by the random pairwise mating, were collected at 4 hpf (hours post fertilization) and incubated in E3 medium, the typically-utilized medium to raise the embryos [45], in 24 well-plates at 28 °C. Embryos were treated by simple soaking or microinjection with different solutions of LIG in E3 medium up to 120 hpf. Concentrations tested were 5, 10, 50 and 100 $\mu g\ ml^{-1}$. E3 medium was used as negative control. The solutions of LIG were replaced with a fresh suspension every 24 h. A set of endpoints, including survival, hatching, heart bate rates and morphological changes, was examined every 24 h (24, 48, 72, 96, 120 hpf) using a stereoscopic microscope (SMZ18, Nikon). The swimming activity of larvae at 96 hpf was recorded with an EthoVision video tracking software (Noldus Information Technology, Wageningen, Netherlands), as previously reported [41]. Experiments were performed in triplicate for statistical accuracy. All animal experiments were performed in full compliance with the revised directive 2010/63/EU.

2.4. Data analysis

All parameters were expressed as mean ± standard deviation and the data were analyzed as previously reported [46].

3. Results and discussion

3.1. Physico-chemical characterization

The LIG obtained by laser-writing of the polyimide film has been deeply characterized from the physico-chemical point of view. As previously described in the literature, its morphology recalls a sponge (figure 1(a) and (b)) with micrometric pores which formed during the laser-induced conversion of the polymer. Specifically, the interaction of the laser with the polyimide film breaks chemical bonds in the polymide repeat units through photothermal effects, promoting the formation of a defective graphenic structure with the simultaneous release of gaseous products [47, 48]. In this way, a three-dimensional porous architecture is obtained, with thins walls (thickness approximately <20 nm) which are constituted by few-layer graphene nanoflakes.

The change in chemical composition induced by the laser process is investigated by XPS: survey spectra and related semi-quantitative analysis confirm that during laser irradiation bonds involving carbon, oxygen and nitrogen are broken, leading to a final structure dominated by carbon atoms (see supporting information (available online at stacks.iop.org/JPhysMaterials/3/034008/mmedia)).

A comparison of high-resolution acquisitions of the C1 s region before and after laser treatment (figure 1(c)) confirms the decrease of oxygen/nitrogen-containing functionalities; moreover, the asymmetric lineshape of the C-C component and the presence of the π–π^* satellite in the C1 s region of LIG give an indication that a graphenic structure is obtained, according to the literature [48, 49].

Further proof of the successful graphenization is provided by TEM analysis, which allows direct investigation of the structure of LIG through high-resolution imaging. Low-magnification TEM images (figure 1(d)) confirm that the LIG flakes are wrinkled and exhibit nanoscale porosity. This is related to the complex structure of the flakes: they are constituted of randomly oriented few-layer graphene domains, as shown in high-resolution TEM images (figure 1(e)), where it is possible to directly visualize the few-layer features, with ≈0.34 nm interplanar spacing characteristic of (002) family of planes in graphite.

Through TEM imaging, it is also possible to estimate the morphology of the LIG flakes after detachment from the substrate for subsequent use in the preparation of dispersions. In this case, it is possible to image single flakes (figure 2(a)) which typically have surface area values <10 μm^2, as shown in the surface area distribution (figure 2(b)) obtained by the analysis of several TEM images of different single flakes.

As a complementary analysis, the same LIG powder, once dispersed in water by sonication was analyzed by dynamic light scattering (DLS) in order to assess the hydrodynamic size dispersion. Figure 2(c) collects the histogram representation of the flake size distribution coming from the DLS measurement, showing that

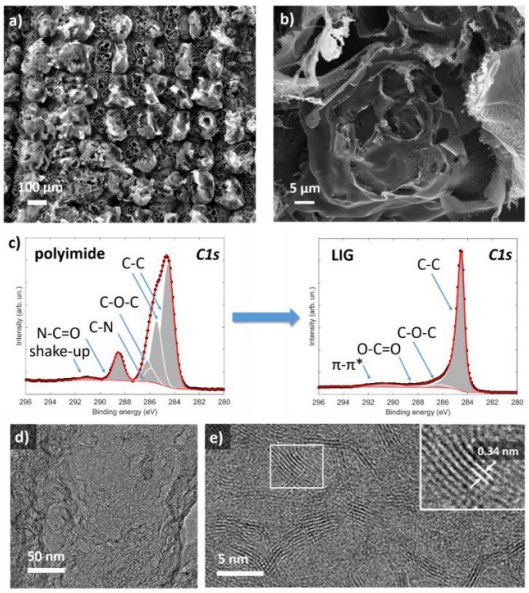

Figure 1. FESEM top-view images (a) and (b) of a laser induced graphene area on polyimide film at different magnifications. (c) provides XPS high-resolution scans of the C1 s region before (left) and after (right) laser treatment. TEM low-magnification image (d) of a LIG nanoflakes, with corresponding high-resolution TEM image (e) providing direct visualization of the structure.

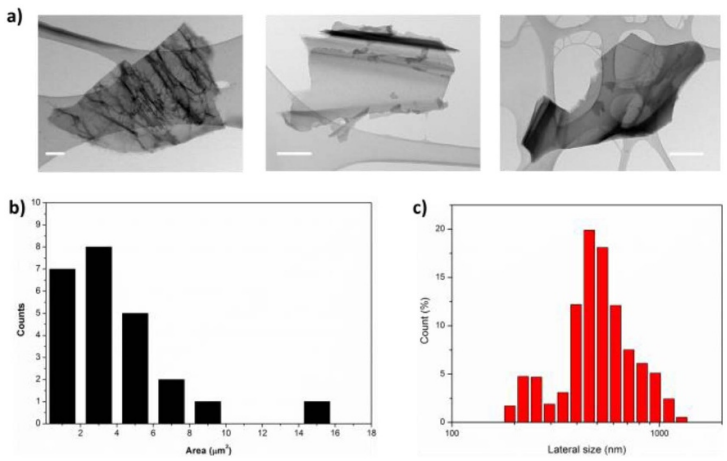

Figure 2. Low magnification TEM images of the morphology of the LIG flakes after detachment from the substrate and sonication (a) and subsequent analysis of the surface area distribution. The scale-bar in TEM images is 500 nm.The distribution of the hydrodynamic size measured by DLS is provided in (c).

the size dispersion is quite broad with not negligible percentage of flakes between 200 ÷ 300 nm or above 1 μm. However, more than 50% of the LIG flakes exhibit an average size of 535 ± 65 nm. It must be stressed that the reported data were calculated using Stokes-Einstein equation [51], representing the effective 'diameter' of the flakes in a spherical geometry approximation; therefore, they cannot be directly correlated with results obtained by the analysis of TEM images.

3.2. Toxicity evaluation

To assess the toxicological profile of laser-induced graphene, embryos were treated with various concentrations of LIG (5, 10, 50 and 100 μg ml^{-1}), and all the toxicological end-points were examined at different time points. The survival and hatching rates were analyzed along the five days of assay (4–120 hpf). The survival rates of zebrafish exposed to laser-induced graphene presented no significant differences at low concentrations of nanomaterials (5 and 10 μg ml^{-1}). At 50 and 100 μg ml^{-1}, the parameter was time and dose-dependent, with a significant decrease in comparison to the control after 72 hpf (figure 3(a)). The hatching time normally corresponds to a temporal window between 48 hpf and 72 hpf. Figure 3(b) showed that the embryos hatched without any delay. Moreover, the hatching rate was time, dose-dependent, and lower than that of the control samples at high LIG concentrations. In accordance with the OECD guidelines

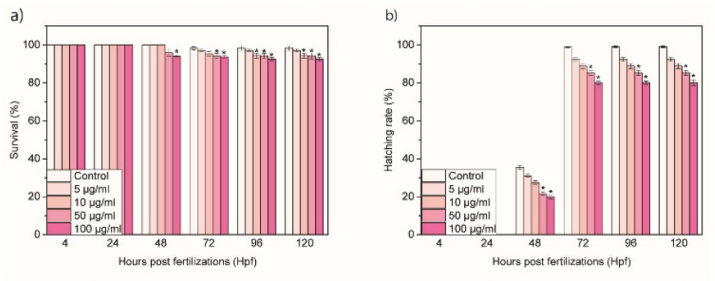

Figure 3. (a) Survival rate and (b) hatching rate of zebrafish after exposure to different concentration of LIG. Data are represented as mean ± SD (standard deviation).

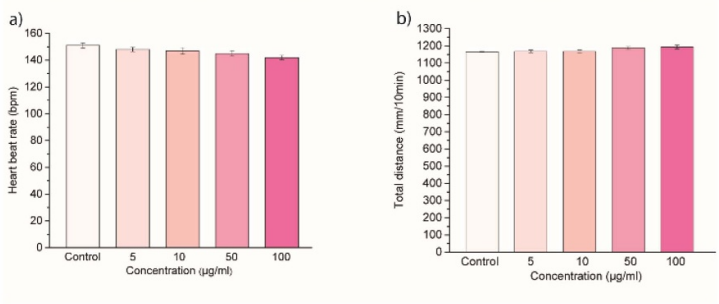

Figure 4. (a) Heart beat rate and (b) total swimming distance of zebrafish after exposure to different concentration of laser-induced graphene. Data are represented as mean ± SD (standard deviation).

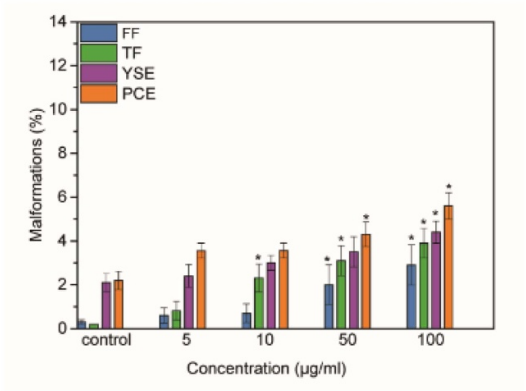

Figure 5. Malformations of zebrafish treated with LIG.

[50], the behavior of these parameters indicated a nontoxic effect of LIG in zebrafish, in contrast to other graphene-family nanomaterials [15, 16].

To determine the possible effects of LIG on larval behavior, we monitored the heart beat rates and the total swimming distances by a visible light test. No considerable changes were detected in the heartbeat rates of larvae of 72 hpf treated with various concentrations of LIG (figure 4(a)). Correspondingly, larvae exposed to laser-induced graphene showed total swimming distances not concentration-dependent and comparable to the control ones (figure 4(b)).

These results indicated no impact of laser-induced graphene on zebrafish larval behavior, with completely different effects compared with other graphene-family nanomaterials [14–16].

Moreover, the treatment of embryos with different concentrations of LIG induced low percentages of abnormalities, even if significant in comparison with the untreated groups (figure 5).

Different well-known anomalies were noted. The yolk sac edema (YSE) and pericardial edema (PCE), finfold flexure (FF) and tail flexure (TF) were the typical deformities induced in embryos and larva treated

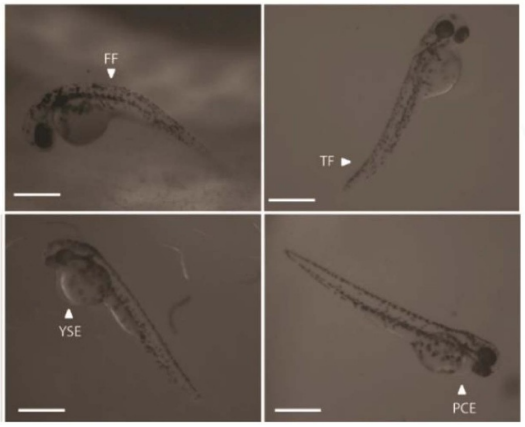

Figure 6. Malformations of zebrafish larvae. FF, finfold flexure, TF, tail flexure, YSE, yolk sac edema, PCE, pericardial edema. Scale bars = 500 μm.

with LIG (figure 6). Similar types of morphological defects in zebrafish embryos/larvae were also caused by other graphene family nanomaterials, such as graphene oxide [16].

In the case of laser-induced graphene, the low percentages of each abnormality confirmed the absence of toxicity of this nanomaterial in zebrafish development.

Our results demonstrate that laser-induce graphene exhibite good biocompatibility in vertebrate systems. These findings are particularly relevant, considering the toxicological profiles of other graphene-family nanomaterials.

Here, we show for the first time, different behavior of laser-induced graphene, that results to be a novel biocompatible platform.

4. Conclusion

In conclusion, we have demonstrated the biosafety of laser-induced graphene in zebrafish, during the different stages of growth. Our results report time and dose-dependent behavior of the survival and hatching rates of embryos and larvae exposed to different concentrations of LIG, with no toxic effects. Moreover, laser-induced graphene has no impact on the swimming and cardiac activities of treated zebrafish, confirming its biocompatibility. In summary, we demonstrate for the first time that laser-induced graphene exhibit a complete different toxicological profile on zebrafish compared to other nanomaterials of the graphene family, including graphene, GO and GO nanosheets. Our results show that laser-induced graphene possesses good biocompatibility, making this nanomaterial a promising platform for several biological applications.

Acknowledgments

S G acknowledges the COST Action CA 15107 'Multi-Functional Nano-Carbon Composite Materials Network (Multi-Comp)'.

ORCID iDs

Andrea Lamberti https://orcid.org/0000-0003-4100-9661
Silvia Giordani https://orcid.org/0000-0002-9212-5067

References

[1] Park S, An J, Jung I, Piner R D, An S J, Li X, Velamakanni A and Ruoff R S 2009 Colloidal suspensions of highly reduced graphene oxide in a wide variety of organic solvents *Nano Lett.* **9** 1593–7
[2] Geim A K 2009 Graphene: status and Prospects *Science* **324** 1530–4
[3] Wang H, Liang Y, Mirfakhrai T, Chen Z, Casalongue H S and Dai H 2011 Advanced asymmetrical supercapacitors based on graphene hybrid materials *Nano Res.* **4** 729–36
[4] Wang H, Cui L F, Yang Y, Sanchez Casalongue H, Robinson J T, Liang Y, Cui Y and Dai H 2010 Mn3O4-graphene hybrid as a high-capacity anode material for lithium ion batteries *J. Am. Chem. Soc.* **132** 13978–80
[5] Pan Y, Sahoo N G and Li L 2012 The application of graphene oxide in drug delivery *Expert Opin. Drug Delivery* **9** 1365–76

[6] Gurunathan S, Han J W, Dayem A A, Eppakayala V and Kim J H 2012 Oxidative stress-mediated antibacterial activity of graphene oxide and reduced graphene oxide in Pseudomonas aeruginosa *Int J Nanomedicine* **7** 5901–14
[7] Zhan S, Zhu D, Ma S, Yu W, Jia Y, Li Y, Yu H and Shen Z 2015 Highly efficient removal of pathogenic bacteria with magnetic graphene composite *ACS Appl. Mater. Interfaces* **7** 4290–8
[8] Tonelli F M, Goulart V A, Gomes K N, Ladeira M S, Santos A K, Lorencon E, Ladeira L O and Resende R R 2015 Graphene-based nanomaterials: biological and medical applications and toxicity *Nanomedicine (Lond)* **10** 2423–50
[9] Sasidharan A, Panchakarla L S, Chandran P, Menon D, Nair S, Rao C N R and Koyakutty M 2011 Differential nano-bio interactions and toxicity effects of pristine versus functionalized graphene *Nanoscale* **3** 2461–4
[10] Chong Y, Ma Y, Shen H, Tu X, Zhou X, Xu J, Dai J, Fan S and Zhang Z 2014 The in vitro and in vivo toxicity of graphene quantum dots *Biomaterials* **35** 5041–8
[11] Liao K H, Lin Y S, Macosko C W and Haynes C L 2011 Cytotoxicity of graphene oxide and graphene in human erythrocytes and skin fibroblasts *ACS Appl. Mater. Interfaces* **3** 2607–15
[12] Akhavan O, Ghaderi E and Akhavan A 2012 Size-dependent genotoxicity of graphene nanoplatelets in human stem cells *Biomaterials* **33** 8017–25
[13] Akhavan O, Ghaderi E, Emamy H and Akhavan F 2013 Genotoxicity of graphene nanoribbons in human mesenchymal stem cells *Carbon* **54** 419–31
[14] Wang Z G *et al* 2015 Toxicity of graphene quantum dots in zebrafish embryo *Biomed. Environ. Sci.* **28** 341–51
[15] Manjunatha B, Park S H, Kim K, Kundapur R R and Lee S J 2018 Pristine graphene induces cardiovascular defects in zebrafish (Danio rerio) embryogenesis *Environ. Pollut.* **243** 246–54
[16] D'Amora M, Camisasca A, Lettieri S and Giordani S 2017 Toxicity assessment of carbon nanomaterials in zebrafish during development *Nanomaterials* **7** 414
[17] Yang K, Gong H, Shi X, Wan J, Zhang Y and Liu Z 2013 In vivo biodistribution and toxicology of functionalized nano-graphene oxide in mice after oral and intraperitoneal administration *Biomaterials* **34** 2787–95
[18] Mao L, Hu M, Pan B, Xie Y and Petersen E J 2016 Biodistribution and toxicity of radio-labeled few layer graphene in mice after intratracheal instillation *Part. Fibre Toxicol.* **13** 7
[19] Ma J, Liu R, Wang X, Liu Q, Chen Y, Valle R P, Zuo Y Y, Xia T and Liu S 2015 Crucial role of lateral size for graphene oxide in activating macrophages and stimulating pro-inflammatory responses in cells and animals *ACS Nano* **9** 10498–515
[20] Duch M C *et al* 2011 Minimizing oxidation and stable nanoscale dispersion improves the biocompatibility of graphene in the lung *Nano Lett.* **11** 5201–7
[21] Ali S, van Mil H G and Richardson M K 2011 Large-scale assessment of the zebrafish embryo as a possible predictive model in toxicity testing *PLoS One* **6** e21076
[22] Ye R, James D K and Tour J M 2018 Laser-induced graphene *Acc. Chem. Res.* **51** 1609–20
[23] Clerici F, Fontana M, Bianco S, Serrapede M, Perrucci F, Ferrero S, Tresso E and Lamberti A 2016 In situ MoS2 decoration of laser-induced graphene as flexible supercapacitor electrodes *ACS Appl. Mater. Interfaces* **8** 10459–65
[24] Peng Z, Ye R, Mann J A, Zakhidov D, Li Y, Smalley P R, Lin J and Tour J M 2015 Flexible boron-doped laser-induced graphene microsupercapacitors *ACS Nano* **9** 5868–75
[25] Ye R, Peng Z, Wang T, Xu Y, Zhang J, Li Y, Nilewski L G, Lin J and Tour J M 2015 In situ formation of metal oxide nanocrystals embedded in laser-induced graphene *ACS Nano* **9** 9244–51
[26] Song W, Zhu J, Gan B, Zhao S, Wang H, Li C and Wang J 2018 Flexible, stretchable, and transparent planar microsupercapacitors based on 3D porous laser-induced graphene *Small* **14** 1702249
[27] Chyan Y and Ye R 2018 Laser-induced graphene by multiple lasing: toward electronics on cloth, paper, and food **12** 2176–83
[28] Nag A, Mukhopadhyay S C and Kosel J 2017 Sensing system for salinity testing using laser-induced graphene sensors *Sensor Actuators* A **264** 107–16
[29] Tao L-Q *et al* 2017 An intelligent artificial throat with sound-sensing ability based on laser induced graphene *Nat. Commun.* **8** 14579
[30] Zhang J, Ren M, Li Y and Tour J M 2018 In situ synthesis of efficient water oxidation catalysts in laser-induced graphene *ACS Energy Lett.* **3** 677–83
[31] Lamberti A, Clerici F, Fontana M and Scaltrito L 2016 A highly stretchable supercapacitor using laser-induced graphene electrodes onto elastomeric substrate *Adv. Energy Mater.* **6** 1600050
[32] Lamberti A, Serrapede M, Ferraro G, Fontana M, Perrucci F, Bianco S, Chiolerio A and Bocchini S 2017 All-SPEEK flexible supercapacitor exploiting laser-induced graphenization *2D Mater.* **4** 035012
[33] Luo J, Fan F R, Jiang T, Wang Z, Tang W, Zhang C, Liu M, Cao G and Wang Z L 2015 Integration of micro-supercapacitors with triboelectric nanogenerators for a flexible self-charging power unit *Nano Res.* **8** 3934–43
[34] Lu Y, Lyu H, Richardson A G, Lucas T H and Kuzum D 2016 Flexible neural electrode array based-on porous graphene for cortical microstimulation and sensing *Sci. Rep.* **6** 33526
[35] Ye R, James D K and Tour J M 2019 Laser-induced graphene: from discovery to translation *Adv. Mater.* **31** 1803621
[36] Singh S P, Li Y, Be'er A, Oren Y, Tour J M and Arnusch C J 2017 Laser-induced graphene layers and electrodes prevents microbial fouling and exerts antimicrobial action *ACS Appl. Mater. Interfaces* **9** 18238–47
[37] d'Amora M and Giordani S 2018 The utility of zebrafish as a model for screening developmental neurotoxicity *Front. Neurosci.* **12**
[38] Lee K J, Browning L M, Nallathamby P D, Desai T, Cherukuri P K and Xu X-H N 2012 In vivo quantitative study of sized-dependent transport and toxicity of single silver nanoparticles using zebrafish embryos *Chem. Res. Toxicol.* **25** 1029–46
[39] Truong L, Harper S L and Tanguay R L 2011 Evaluation of embryotoxicity using the zebrafish model *Methods Mol. Biol.* **691** 271–9
[40] McAleer M F, Davidson C, Davidson W R, Yentzer B, Farber S A, Rodeck U and Dicker A P 2005 Novel use of zebrafish as a vertebrate model to screen radiation protectors and sensitizers *Int. J. Radiat. Oncol. Biol. Phys.* **61** 10–13
[41] Brannen K C, Panzica-Kelly J M, Danberry T L and Augustine-Rauch K A 2010 Development of a zebrafish embryo teratogenicity assay and quantitative prediction model *Birth Defects Res. B Dev. Reprod. Toxicol.* **89** 66–77
[42] Hill A J, Teraoka H, Heideman W and Peterson R E 2005 Zebrafish as a model vertebrate for investigating chemical toxicity *Toxicol. Sci.* **86** 6–19
[43] d'Amora M and Giordani S 2018 *Smart Nanoparticles for Biomedicine*, ed G Ciofani (Amsterdam: Elsevier) pp 103–13
[44] Nunn N *et al* 2018 Fluorescent single-digit detonation nanodiamond for biomedical applications *Methods. Appl. Fluoresc.* **6** 035010
[45] d'Amora M, Cassano D, Pocoví-Martínez S, Giordani S and Voliani V 2018 Biodistribution and biocompatibility of passion fruit-like nano-architectures in zebrafish *Nanotoxicology* **12** 914–22

[46] Lin J, Peng Z, Liu Y, Ruiz-Zepeda F, Ye R, Samuel E L G, Yacaman M J, Yakobson B I and Tour J M 2014 Laser-induced porous graphene films from commercial polymers *Nat. Commun.* **5** 5714
[47] Lamberti A, Perrucci F, Caprioli M, Serrapede M, Fontana M, Bianco S, Ferrero S and Tresso E 2017 New insights on laser-induced graphene electrodes for flexible supercapacitors: tunable morphology and physical properties *Nanotechnology* **28** 174002
[48] Yang D Q and Sacher E 2006 Carbon 1s X-ray photoemission line shape analysis of highly oriented pyrolytic graphite: the influence of structural damage on peak asymmetry *Langmuir* **22** 860–2
[49] Matthew J 2004 Surface analysis by Auger and X-ray photoelectron spectroscopy. D Briggs and J T Grant (eds). IMPublications, Chichester, UK and SurfaceSpectra, Manchester, UK, 2003. 900 pp., ISBN 1-901019-04-7, 900 pp *Surf. Interface Anal.* **36** 1647
[50] Busquet F, Halder M, Braunbeck T, Gourmelon , Lillicrap A, Kleensang A, Belanger S, Carr G and Walter-rohde S 2013 *OECD GUIDELINES FOR THE TESTING OF CHEMICALS 236 - Fish Embryo Acute Toxicity (FET) Test*
[51] Arenas-Guerrero P, Delgado Á V, Donovan K J, Scott K, Bellini T, Mantegazza F and Jiménez M L 2018 Determination of the size distribution of non-spherical nanoparticles by electric birefringence-based methods *Sci. Rep.* **8** 9502